Potential for Mineral Carbonation of CO_2 in Pleistocene Basaltic Rocks in Volos Region (Central Greece)

Nikolaos Koukouzas [1],*, Petros Koutsovitis [2], Pavlos Tyrologou [1] , Christos Karkalis [1,3] and Apostolos Arvanitis [4]

[1] Centre for Research and Technology, 15125 Hellas (CERTH), Greece; tyrologou@certh.gr (P.T.); karkalis@certh.gr (C.K.)

[2] Section of Earth Materials, Department of Geology, University of Patras, GR-265 00 Patras, Greece; pkoutsovitis@upatras.gr

[3] Department of Mineralogy and Petrology, Faculty of Geology and Geoenvironment, National and Kapodistrian University of Athens, Zografou, P.C. 15784 Athens, Greece

[4] Hellenic Survey of Geology and Mineral Exploration (HSGME), 13677 Attica, Greece; arvanitis@igme.gr

* Correspondence: koukouzas@certh.gr; Tel.: +30-211-106-9502

check for updates

Abstract: Pleistocene alkaline basaltic lavas crop out in the region of Volos at the localities of Microthives and Porphyrio. Results from detailed petrographic study show porphyritic textures with varying porosity between 15% and 23%. Data from deep and shallow water samples were analysed and belong to the Ca-Mg-Na-HCO_3-Cl and the Ca-Mg-HCO_3 hydrochemical types. Irrigation wells have provided groundwater temperatures reaching up to ~30 °C. Water samples obtained from depths ranging between 170 and 250 m. The enhanced temperature of the groundwater is provided by a recent-inactive magmatic heating source. Comparable temperatures are also recorded in adjacent regions in which basalts of similar composition and age crop out. Estimations based on our findings indicate that basaltic rocks from the region of Volos have the appropriate physicochemical properties for the implementation of a financially feasible CO_2 capture and storage scenario. Their silica-undersaturated alkaline composition, the abundance of Ca-bearing minerals, low alteration grade, and high porosity provide significant advantages for CO_2 mineral carbonation. Preliminary calculations suggest that potential pilot projects at the Microthives and Porphyrio basaltic formations can store 64,800 and 21,600 tons of CO_2, respectively.

Keywords: basalts; carbonation; CO_2 storage; hydrochemistry; regional heat flow

1. Introduction

The use of fossil fuels (coal and oil) in the industries has increased the CO_2 emissions in the atmosphere. Anthropogenic CO_2 is a major greenhouse gas that contributes to the change of climate [1,2]. To mitigate the problem of global warming, several technologies have been developed. CO_2 Capture and Storage (CCS) is one of the most advanced technologies that mediates the increase of the CO_2 contents in the atmosphere [3]. Basaltic rocks exhibit appropriate physicochemical properties for the implementation of carbonate mineral precipitation, through interaction of the Ca-Mg-Fe rich minerals with carbonic acid, derived from the dissolution of the injected CO_2 in water [4]. The newly formed minerals mostly consist of calcite, magnesite and siderite [5,6], which provide the potential for long-term and safe storage. Selection of the appropriate type of basalt and region for implementing CO_2 storage techniques via mineral carbonation requires detailed mineralogical and petrophysical (porosity, permeability) studies. The nature of the injected CO_2 affects the integrity and trapping potential of

the rock material [7]. CO_2 is present in the supercritical form (sCO_2) at pressure and temperature conditions that correspond to depths greater than 1 km. In such environments, sCO_2 can give rise to various geochemical reactions, causing the dissolution/precipitation of primary and secondary minerals, as well as changes in porosity and permeability properties [8,9]. Successful CCS pilot injection projects have been implemented, including the sites Ferrybridge (UK), Aberthaw Pilot Plant (UK), Puertollano (Spain), Ketzin (Germany), and Hvergerdi (Iceland; CarbFix project) [10].

Alkali basaltic rocks with the potential of CO_2 storage are relatively restricted but widespread throughout mainland Greece [10]. Main areas of basalt appearance are located in the regions of Pindos (NW Greece; [11]), Central and Southern Aegean islands [12–14], Koziakas [15], Othris [16], Evia island [17], and Argolis [18]. The present study focuses on studying the Porphyrio and Microthives alkali basaltic outcrops for their mineralogical potential of CO_2 sequestration. The study areas are located 8 and 12 km south-southwest of the industrial city of Volos, respectively (Figure 1). These volcanic rocks formed along with other adjacent scattered volcanic centers that were active during the Late Pleistocene–Quaternary period, including the islands of Lichades, Achilleio, and Agios Ioannis between the gulfs of Pagasitikos and North Evoikos. Their formation is attributed to back-arc extensional volcanism and affected by the activity of the Northern Anatolian fault [19–21]. They comprise massive lavas and pyroclastic rocks that include basaltic rock fragments and pumice. These volcanic rock formations are located in the Pelagonian Zone and the Eohellenic tectonic nappe [22,23]. The Pelagonian Zone is part of the Internal Hellinides, and it can be distinguished into two metamorphic and non-metamorphic groups, respectively [24,25]. It was over-thrusted by the Eohellenic nappe during the Late Jurassic to Early Cretaceous period [24,26]. In the studied regions, the Pelagonian Zone mostly consists of clastic sedimentary rocks, limestones, and ophiolitic occurrences [22,23]. The Eohellenic tectonic nappe consists mainly of metamorphosed sedimentary rocks, serpentinites, and ophicalcites [22,23], as well as gneissic formations of the Volos Massif [21], composed of gneiss, muscovite, and mica-chlorite schists.
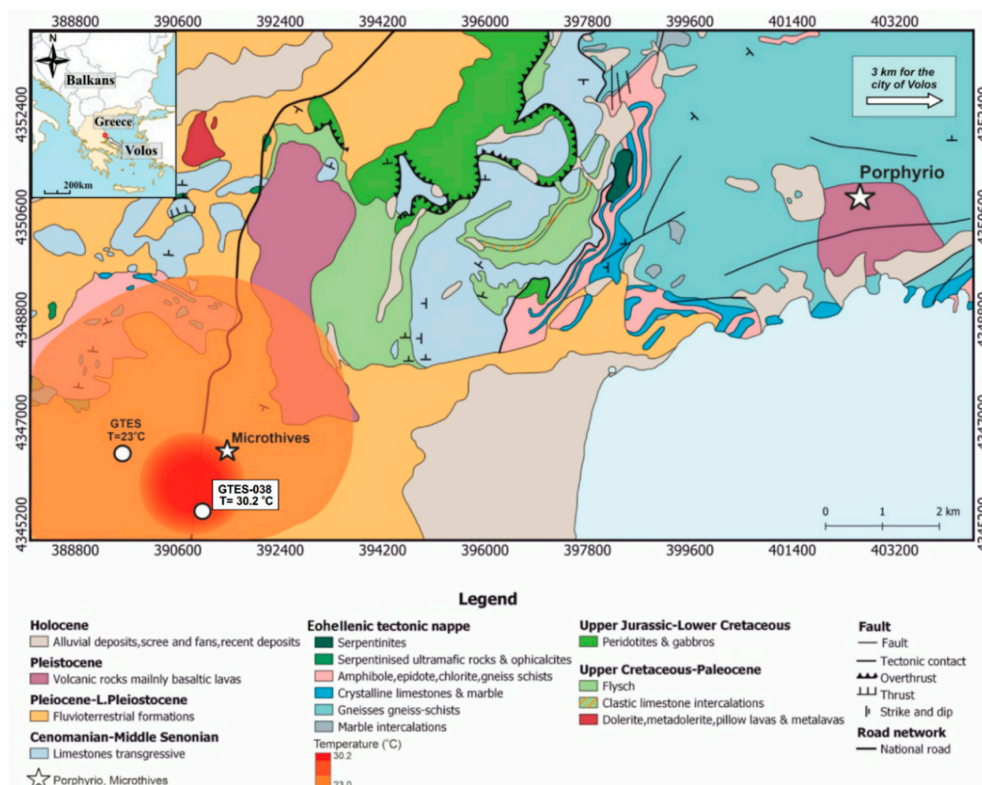
Figure 1. Geological map of Microthives locality and calculated water temperatures, EGSA87.

This study presents new mineralogical, mineral chemistry, and petrographic data of the volcanic rocks from the localities of Microthives and Porphyrio, coupled with hydrochemical data of groundwater samples from irrigation wells, to estimate their potential for the development of geological carbon capture and storage (CCS) [27]. The present study focuses on examining the physicochemical features necessary for applying CCS technologies focusing on: (i) degree of alteration, (ii) nature and geochemistry of the basalts, (iii) presence of Ca-bearing minerals, (iv) porosity (v), indications of enhanced heat calculated in groundwater samples from irrigation wells, and (vi) locality advantages.

2. Materials and Methods

This study includes the investigation of rocks that have been collected from the region of Volos (Central Greece; SE Thessaly), focusing on the volcanic occurrences of the Porphyrio and Microthives localities. Sampling was carried out to select the most appropriate rocks regarding their porosity and mineralogical assemblage. Modal composition of pores was calculated by applying ~500 counts on each thin section. Calculations were cross-correlated with image analysis techniques performed on the same thin sections. More than 50 rock samples were examined through detailed petrographic observations upon polished thin sections with the use of a Zeiss Axioskop-40 (Zeiss, Oberkochen, Germany), equipped with a Jenoptik ProgRes CF Scan microscope camera at the Laboratories of the Center for Research and Technology, Hellas (CERTH). Mineral chemistry analyses were conducted at CERTH using a SEM–EDS JEOL JSM-5600 scanning electron microscope (Jeol, Tokyo, Japan), equipped with an automated energy dispersive analysis system ISIS 300 OXFORD (Oxford Instruments, Abington, UK), with the following operating conditions: 20 kV accelerating voltage, 0.5 nA beam current, 20 s time of measurement, and 5 μm beam diameter. SEM-EDS facility was calibrated to obtain accurate quantitative results using standard reference materials. In order to perform standardised quantitative analyses, thin sections were flat, polished, and carbon coated. XRD analyses were conducted at CERTH using a Philips X'Pert Panalytical X-ray diffractometer (Malvern Panalytical, Malvern, UK), operating with Cu radiation at 40 kV, 30 mA, 0.020 step size, and 1.0 sec step time. For the evaluation of the XRD patterns, DIFFRAC plus EVA software v.11 was deployed (Bruker, MA, USA) based on the ICDD Powder Diffraction File (2006). Physicochemical data (from the Hellenic Survey of Geology and Mineral Exploration (HSGME)) [28], including temperature and pH values, are also provided for two groundwater samples from local irrigation wells (sample GTES-038; 250 m depth, sample GTES-040; 180 m depth).

3. Results

3.1. Petrography and Mineral Chemistry

Basalts from Microthives and Porphyrio localities exhibit porphyritic, vesicular textures. The groundmass is fine-grained holocrystalline, being either trachytic or aphanitic (Figure 2a–f) and often enriched in oxide minerals (ilmenite and magnetite). The porosity, after the examination of an extended number of thin sections of basaltic rock samples ($n > 50$), varies highly from 5 to 40% in the more massive and porous samples, respectively. The vast majority, though, were determined to have porosity that ranges from 15% to 23% (Avg. 18%). Vesicles are in cases filled with secondary calcite.

Their mineralogical assemblage is predominantly composed by prismatic subhedral and rarely euhedral clinopyroxene (15–30%) and olivine (10–20%) phenocrysts (450–700 μm diameter), enclosed within a clinopyroxene and plagioclase-rich groundmass (50–60%). Plagioclase is mostly restricted in the groundmass, appearing in the form of needle- to lath-shaped crystals that compositionally are either bytownite and labradorite ($An_{68.9-71.6}$). Accessory minerals (<5%) include alkali-feldspar, quartz, calcite, amphibole, orthopyroxene, apatite, opaque minerals (ilmenite, titanomagnetite, and magnetite), and pyrite.
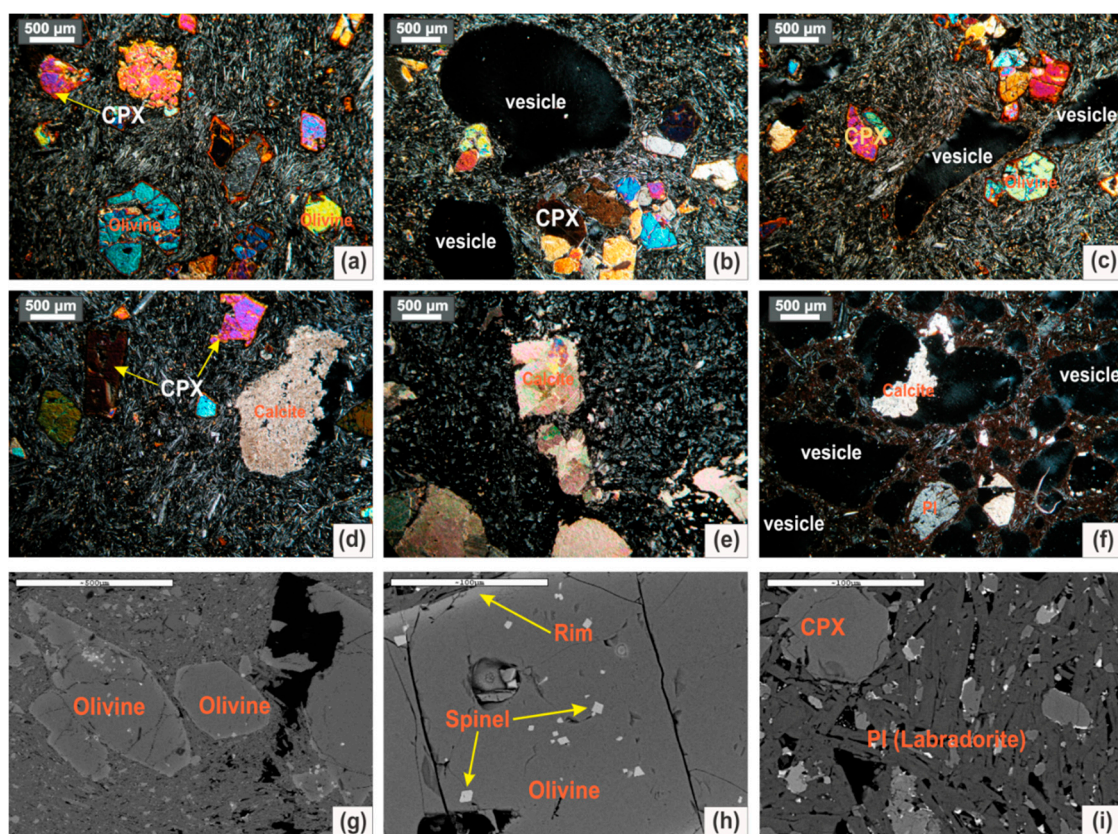
Figure 2. (**a**) Olivine and clinopyroxene phenocrystals in a hypo-crystalline trachytic groundmass mostly consisting of lath-shaped plagioclase but also K-felspar (Sample M3). (**b**,**c**) Vesicular basaltic lava samples M1 and M8, mainly consisting of clinopyroxene and also olivine phenocrystals, exhibiting glomeroporphyritic textures. It includes a hypo-crystalline trachytic groundmass, as well as vesicular textures. (**d**) Vesicular basaltic lava sample M2, with clinopyroxene and olivine phenocrystals in a trachytic groundmass. Vesicles are occasionally filled with secondary calcite-forming amygdaloidal textures. (**e**) Vesicular basaltic lava sample M5, within a microcrystalline vesicular groundmass, filled with secondary calcite. (**f**) Pyroclastic tuff with a high percentage of vesicles. Groundmass locally aphanitic with rare feldspar phenocrysts. (**g**–**i**) BSE (Back Scattered Electron) images with olivine and clinopyroxene phenocrysts.

Clinopyroxene is mainly classified as augite and less often as diopside, displaying highly variable TiO_2 and Al_2O_3 contents (0.55–2.94 wt.% and 2.22–7.69 wt.%, respectively). SiO_2 contents range between 44.52 and 51.34 wt.%. Representative compositions of olivine are presented in Table 1. They contain 38.10–40.55 wt.% SiO_2 and variable FeO and MgO contents (10.30–24.90 wt.% and 36.58–48.50 wt.%, respectively). Mg# ranges between 72.78 and 89.36 wt.%.

The mineralogical composition of the studied basaltic rocks was also investigated by powder X-ray diffraction (XRD). In accordance with petrographic observations and mineral chemistry results, the main mineral phases were confirmed with XRD patters, based upon the DIFFRACplus EVA software (version11, Bruker, MA, USA) recommendations. In particular, the peaks at ~51.0° 2θ correspond to the olivine porphyroblasts, whereas clinopyroxene corresponds to peaks at 29.80–30.80° 2θ. The presence of magnetite in small amounts is characterised by small peaks at ~30° 2θ, ~52° 2θ and 62.20–62.80° 2θ. The plagioclase crystals of the basaltic groundmass were recognised by the peaks at ~28.0° 2θ, ~22.0° 2θ, and ~24.30° 2θ.

Table 1. Representative mineral chemistry analyses. (Abbreviations: Ol: olivine, Cpx: clinopyroxene, Plg: plagioclase, K-fs: K-feldspar, Amph: amphibole, Opx: orthopyroxene, Spl: spinel, n: number of analysis, Mg# = 100 × molar MgO/(MgO + FeO$_t$), Cr# = 100 × molar Cr$_2$O$_3$/(Cr$_2$O$_3$ + Al$_2$O$_3$).)

Min. Sample n:	Ol M3 7	Ol M3 1	Ol M3 5	Ol M7 2	Cpx M3 3	Cpx M3 4	Cpx M7 1	Cpx M7 1	Cpx M3 1	Plg M3 2	Plg M7 4
SiO$_2$	40.55	39.04	38.1	39.61	50.23	51.34	49.96	49.06	44.52	50.34	49.15
TiO$_2$	0.03	0.04	0.14	0.14	1.27	0.55	1.17	1.58	2.94	0.12	0.14
Al$_2$O$_3$	0.02	0.04	0.03	0.06	4.16	2.22	5.22	4.46	7.69	31.6	32.57
FeO	10.3	17.62	24.39	14.14	5.64	5.79	5.37	6.05	8.17	0.46	0.57
MnO	0.16	0.13	0.2	0.13	21.66	21.77	21.58	23.16	23.57	13.84	14.34
MgO	48.5	42.33	36.58	45.48	15.9	17.07	15.32	14.4	11.88	-	-
CaO	0.15	0.38	0.45	0.13	21.66	21.77	21.58	23.16	23.57	13.84	14.34
Na$_2$O	-	-	-	-	0.5	0.62	0.68	0.66	0.74	3.3	2.92
K$_2$O	-	-	-	-	0.09	0.03	0.07	0.06	0.74	3.3	2.92
Cr$_2$O$_3$	0.03	0.04	0.05	0.04	0.22	0.41	0.38	0.49	0.02	-	-
NiO	0.29	0.13	0.12	0.24	0.03	0.07	0.02	0.05	0.05	-	-
Total	100.02	99.75	100.07	99.94	99.93	100.03	99.9	100.08	99.81	99.88	100.02
Mg#	89.36	81.07	72.78	85.15							

Min. Sample n:	K-fs M3 4	K-fs M5 1	Amph M3 1	Amph M3 1	Opx M3 5	Glass M7 2	Min. Sample n:	Spl M3 3	Spl M3 1	Spl M3 2
SiO$_2$	65.38	64.5	51.59	53.78	53.02	57.09	Cr$_2$O$_3$	35.56	23.72	30.36
TiO$_2$	0.07	0.06	0.47	0.3	0.7	1.65	Al$_2$O$_3$	31.27	43.51	22.35
Al$_2$O$_3$	18.75	18.7	23.35	27.68	0.78	17.53	TiO$_2$	0.93	0.5	4.21
FeO	0.23	0.54	2.34	0.57	17.85	4.27	FeO	16.82	14.14	33.27
MnO	-	-	0.04	0.11	0.85	0	MgO	14.56	16.72	8.91
MgO	-	-	4.32	0	23.95	2.25	MnO	0.05	0.09	0.23
CaO	0.27	0.15	11.66	9.81	2.46	6.84	NiO	0.19	0.18	0.13
Na$_2$O	4.03	3.57	2.5	3.76	0	3.02	SiO$_2$	0.43	0.7	0.39
K$_2$O	11.02	12.02	0.49	1.47	0.1	6.91	Total	99.81	99.56	99.82
Cr$_2$O$_3$	-	-	0.31	0.02	0.15	0.36				
NiO	-	-	0.26	0.07	0.13	0.08	Mg#	62.08	67.56	37.6
Total	99.75	99.54	97.33	97.55	99.99	100	Cr#	43.26	26.77	47.67

3.2. Rock Classification and Geochemistry

Volcanic rocks from the region of Volos correspond to small scattered outcrops with an age range from 0.5 to 3.4 Ma [21,29]. Their formation was attributed to Pleistocene back-arc extension in the Aegean Sea [19,30,31]. Based upon the total alkali–silica (TAS) diagram (Figure 3a), the extensional-related volcanic rocks from the Volos plot formed within the basaltic trachyandesite and trachyandesite fields. Pleistocene basalts from the adjacent regions of Kamena Vourla, Lichades islands, Psathoura, and Achilleio also plot in the same compositional fields (Figure 3a). Chondrite-normalised REE patterns of the Volos basaltic rocks (Figure 3b) are highly enriched in LREE (La/Yb$_{CN}$ = 0.34–0.44) and also present notable negative Eu anomalies (Eu$_{CN}$/Eu* = 0.73–0.80), with the later implying plagioclase fractionation. These are additionally characterised from trace element ratios that account for a clear OIB (Ocean Island Basalt)-signature: Zr/Nb = 4.66–19.82, La/Nb = 0.75–10.38, and Ba/Th = 39.4–100.95 [32]. Basalts from the aforementioned adjacent regions exhibit lower LREE enrichments (Figure 3b), indicating higher degrees of partial melting and/or differentiation processes.

The Pleistocene extensional-related basaltic rocks from Volos and the adjacent regions differ from other recent age (Pliocene–present) volcanic rocks in Greece. The latter are subduction-related volcanics from the South Aegean (Methana [26,33], Nisyros [34], and Santorini [2,35,36]), associated with the subduction of the African plate beneath Eurasia [37–39]. These compositionally correspond to subalkaline basalts and andesites (Figure 3a), which possess significantly lower LREE and also higher HREE contents (Figure 3b). From this comparison, it is evident that the basaltic rocks from Volos

are among the very few alkaline basaltic rocks of recent age that are compositionally suitable for considering mineral carbonation of CO_2.
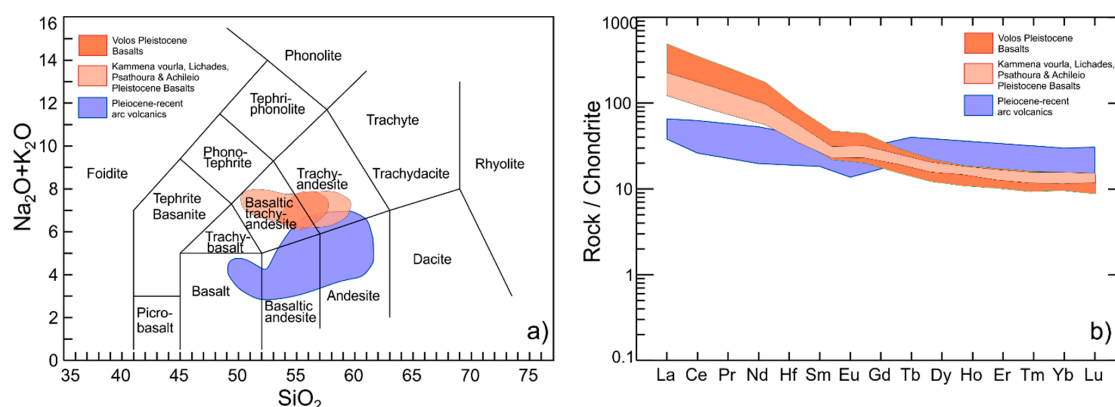
Figure 3. (**a**) Total alkali–silica (TAS), $Na_2O + K_2O$ vs. SiO_2 [40], and (**b**) chondrite-normalised REE patterns [41,42] of volcanic rocks from Volos, Kamena Vourla, Psathoura, Achilleio, Lichades [21], Methana [26,33], Nisyros island [34], and Santorini island [2,35,36].

3.3. Water Chemistry and Temperature Data

Geothermal data from the Almyros–Microthives basin [28] indicate that the north part of the basin is characterised by Pleistocene volcanic activity. Deep groundwater (sample GTES-038; >250 m depth) exhibits a temperature of 30.2 °C and a pH of 7.30, whereas shallow groundwater (sample GTES-040; probably 170–180 m depth) presents a temperature of 23.0 °C and a pH of 7.40. The elevated water temperatures appear in the vicinity of the basaltic dominated areas. Based on the Castany classification [43], the analysed groundwaters belong to hypothermal, neutral-to-alkaline types. Their total dissolved solids (TDS) content is 660 mg/L (Table 2). TDS calculation was based on the cations and anions sum, including HCO_3^- (0.49 ×(HCO_3^-)) and B. The total hardness values are 309 and 363 mg/L for the deep and shallow groundwaters, respectively. Non-carbonated hardness values are 22 and 0 mg/L for the deep and shallow groundwater samples, respectively.

Table 2. Hydrochemical analyses of groundwater samples from Microthives locality [28]. *T* (°C); conductivity (µS/cm); concentrations (mg/L); total dissolved solids (TDS) (mg/L).

Sample	*T*	pH	Cond.	TDS	Ca	Mg	Na	K	CO₃	HCO₃	Cl	SO₄	NO₃	SiO₂
GTES-038	30.2	7.70	989.0	660	55.30	41.70	80.50	2.25	0.00	287.0	165	24.60	0.00	34.90
GTES-040	23.0	7.60	693.0	460	38.70	65.10	17.60	1.30	0.00	437.0	19.50	9.80	3.72	56.0

From the Hem [44] and Sawyer and McCarty [45] classifications, the analysed groundwater samples are classified as very hard. Deep and shallow groundwater samples belong to the Ca-Mg-Na-HCO_3-Cl and the Mg-HCO_3 hydrochemical types, respectively (Figure 4).

Hydrogeochemical comparisons between the two water samples from Microthives and Aegean seawater [47], are discussed below (see Discussion paragraph).
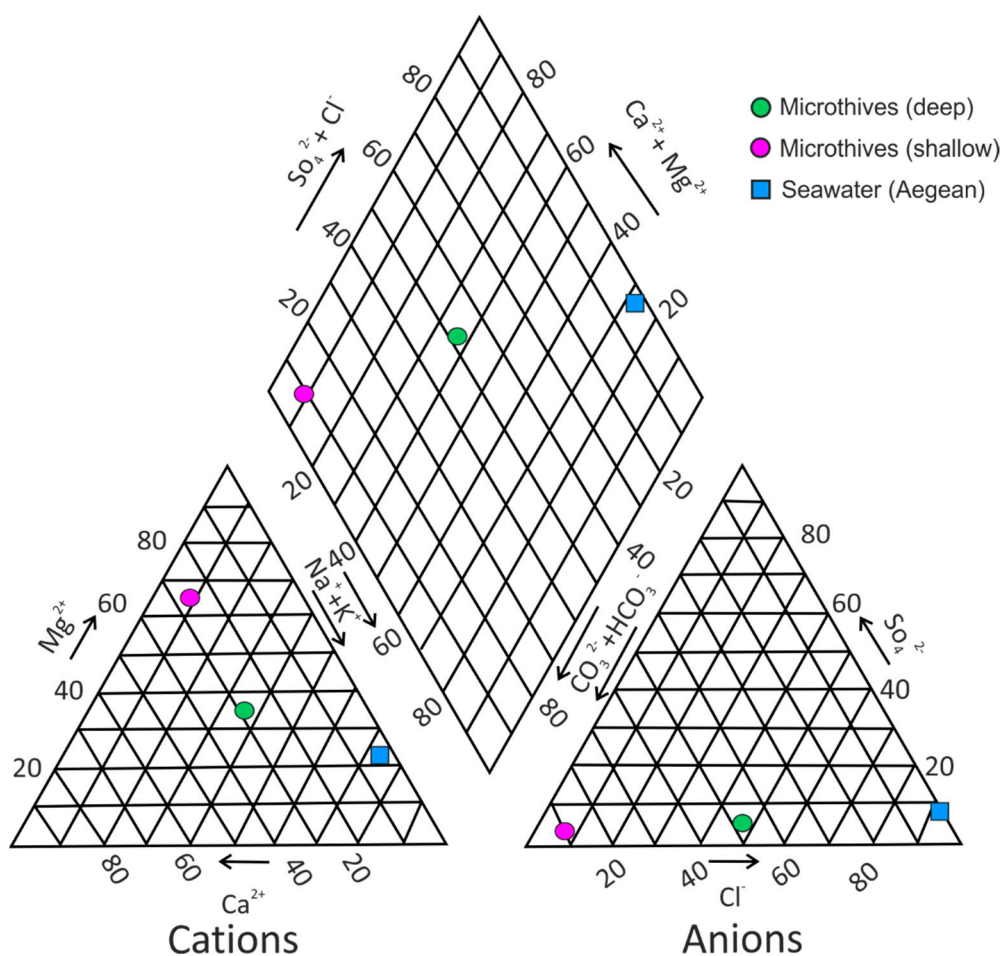
Figure 4. Piper diagram [46] for the water samples of Microthives and Aegean regions.

4. Discussion

4.1. Mineral Reactions

Despite the high availability of basalts on the Earth's surface [48–50], only few basaltic types have the appropriate petrophysical and chemical properties [3,6,50–52] to serve as host rocks suitable for CO_2 mineral carbonation. The basaltic rocks from the localities of Porphyrio and Microthives possess proper mineralogical, chemical, and textural features to apply CO_2 sequestration techniques. These features include the high abundance of Ca-bearing minerals, as well as their silica-undersaturated alkaline composition and high porosity. Mineral chemistry reactions that result from this interaction can be modeled based on data provided from this study.

The physicochemical properties of water strongly affect the formation of carbonate minerals during the interaction of basalts with the CO_2 injected fluids. Carbonation with the presence of water can lead to higher amounts of sequestered CO_2 compared to the dry carbonation processes [53,54]. The dissolution of CO_2 in water further affects the liquid reactivity, due to the high amounts of the released H^+ [3,4,6,50]. The concentration of Mg in water can affect the crystal growth of calcite, whereas, at high temperatures, Mg can precipitate in the form of solid mineral phases [3]. In addition, the water saturation reflected from the water/rock ratio (W/R) determines the dissolution of basaltic rocks, which is higher in CO_2 saturated solutions compared to the undersaturated ones (W/R: 10/1 and 2/1 respectively; atmosphere [3]).

The underground water analysed from the region of Microthives is classified as neutral to alkaline (pH = 7.30). Dissolution of CO_2 in water produces carbonic acid. The gradual mixing of the alkaline groundwater with the acidic injection fluids starts up with the entrance of the injected fluid into the

storage formation and ends up with the entrance of the fluid in the monitoring wells [55]. After the mixing process, the formation fluids become more acidic, presenting lower pH values [55]. This acidic pH is characterised by a high concentration of dissolved inorganic carbon (DIC), making the water reactive with the basaltic rocks, due to the high H^+ contents [50].

Addition of CO_2 is expected to lower the pH of water due to the release of H^+ ions, according to the following chemical reactions [50]:

$$CO_2 + H_2O = H_2CO_3 \tag{1}$$

$$H_2CO_3 = HCO_3^- + H^+ \tag{2}$$

Basaltic rocks are rich in Ca, Mg, and Fe, providing the potential for CO_2 mineralisation in the form of carbonate minerals. The released H^+ ions (chemical reaction-2) increase the reactivity of water, resulting in dissolution of the primary basalt minerals and the precipitation of Ca^{2+}, Mg^{2+}, and Fe^{2+} in the form of carbonate minerals [4,50], according to the following chemical reaction:

$$(Ca,Mg,Fe)^{2+} + H_2CO_3 \rightarrow (Ca,Mg,Fe)CO_3 + 2H^+ \tag{3}$$

Carbonation of olivine is described by mineral reaction-4. The high MgO contents (MgO: 36.58–48.50%) of the studied olivine phenocrysts will produce high amounts of magnesite. This reaction is developed with slow rates in the natural systems, suggesting that the carbonation of olivine must be enhanced by a large-scale storage method for CO_2 mineralisation [56,57]. The formation of hydromagnesite is favoured at low temperatures and can be described by reaction-5 [58]. At low temperatures ($T < 60\,°C$), indirect precipitation of magnesite can occur via hydromagnesite dehydration [58]. This process is described through the two-way reaction-6 [59].

$$Mg_2SiO_{4(s)} + 2CO_2 \rightarrow 2MgCO_{3(s)} + SiO_{2(s)} \tag{4}$$

$$5Mg_2SiO_{4(s)} + 8CO_{2\,(gas)} + 2H_2O_{(liq.)} \rightarrow 2\,(4MgCO_3 \cdot Mg(OH)_2 \cdot 4H_2O)_{(s)} + 5H_4SiO_{4(aq)} \tag{5}$$

$$4Mg(CO_3) \cdot Mg(OH)_2 \cdot 4H_2O \leftrightarrow 4MgCO_3 + Mg(OH)_2 + 4H_2O \tag{6}$$
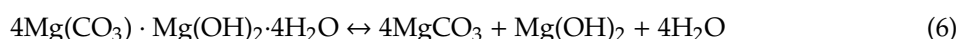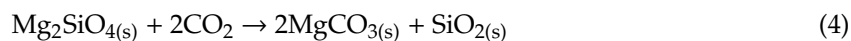
The studied olivine crystals of Microthives and Porphyrio basalts are mostly composed by forsterite. In that case, the olivine carbonation can be further described by the following mineral reaction:

$$Mg_2SiO_{4(s)} + 4H^+_{(aq)} \rightarrow 2Mg^{2+} + SiO_{2(s)} + 2H_2O \tag{7}$$

Dissolution of clinopyroxene is developed according to the following mineral reaction:

$$MgCaSi_2O_6 + 4H^+ \rightarrow Mg^{2+} + Ca^{2+} + 2H_2O + 2SiO_{2(aq)} \tag{8}$$
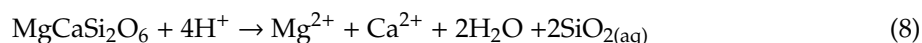
The release of Ca^{2+} cations is described by the dissolution of anorthite rich plagioclase according to the chemical reaction-9:

$$CaAl_2Si_2O_8 + 8H^+ \rightarrow Ca^{2+} + 2Al^{3+} + 4H_2O + 2SiO_{2(aq)} \tag{9}$$
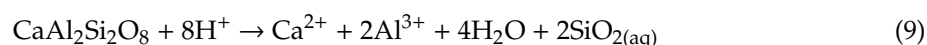
Orthopyroxene appears in the form of accessory enstatite crystals. Dissolution of enstatite is described by mineral reaction-10 [60]:

$$MgSiO_3 + 2H^+ \rightarrow Mg^{2+} + SiO_2 + H_2O \tag{10}$$
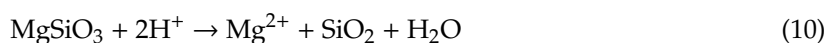
Precipitation of calcite (reaction-11 [50]) during hydrothermal alteration of basaltic rocks is strongly associated with temperature and depth. The Ca^{2+} required for calcite precipitation is mostly derived from the primary calc–silicate minerals and the glass matrix of the basaltic protolith. These minerals mostly include clinopyroxene (CaO: 21.58–23.57%), plagioclase (CaO: 13.84–14.34%), and amphiboles (CaO: 9.81–11.66%).

$$Ca^{2+} + CO_2 + H_2O \rightarrow CaCO_3 + 2H^+ \tag{11}$$

Calcite formation is not favoured at temperatures higher than 290 °C [61] and depths between 200 and 400 m [62]. The time required for carbonate minerals precipitation strongly depends on the abundance of divalent cations, the fluid *P–T*, the liquid chemistry, the CO_2 saturation, and the pore surface area [4]. Diagrams of basalt dissolution rates vs. pH (Figure 5a,b) were designed using data from the literature [50,63–65]. The aforementioned diagrams indicate that during the mixing of the background water with the CO_2 injected fluids, the pH decrease enhances the dissolution rate of forsterite (Mg-olivine) and augite (clinopyroxene). The crystalline basalts in Microthives and Porphyrio localities are mostly composed by clinopyroxene and olivine phenocrystals within a glass-rich matrix. Clinopyroxene is mostly classified as augite, whereas olivine is characterised by relatively high MgO contents (Table 1). The glass-rich basalts are characterised by relatively constant dissolution rates for pH values between 4 and 7.3, whereas their dissolution rates increase with further pH decrease. For pH values lower than 4, the dissolution rate will be rapidly increased and become similar with that of forsterite. This indicates that during the initial stages of the CO_2 injection, more glass-rich basalts will be dissolved with lower rates compared to the crystalline ones. During the interaction of Microthives and Porphyrio basalts with CO_2 injected fluids, clinopyroxene-olivine porphyroblasts [3,6,50,66] and the anorthite-glass rich matrix will be dissolved with similar rates against their pH [3,6,50,67]. The aforementioned results indicate that clinopyroxene and olivine porphyroblasts will be the first mineral phases to be dissolved during the CO_2 injection.
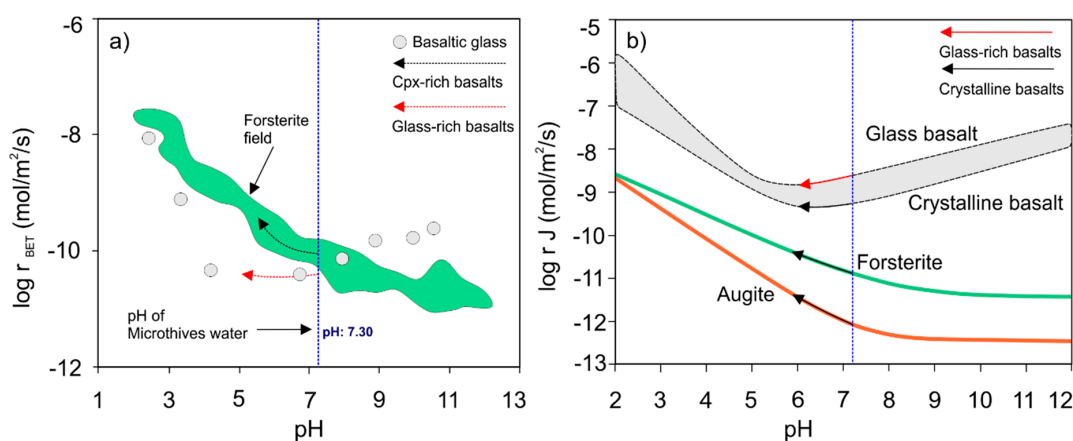
Figure 5. (**a**) Modified diagram of the dissolution rate of the forsterite (*T*: 25 °C; [64]) and basaltic glass (*T*: 30 °C) [65] vs. pH. The dissolution rate is normalised to the BET surface area of the dissolving mineral and glass grains. (**b**) Modified diagram [68] of the dissolution fluxes (mol m^{-2} s^{-1}) at *T*: 25 °C of crystalline and glassy basalts. Forsterite and augite dissolution rates taken from [63].

Based on the experimental results from Gislason et al. [50] (Figure 5a), the dissolution rate of olivine increases from 10^{-10} to $10^{-8.5}$ (mol/m^2/s) for pH values ranging from 7.3 (Microthives water pH) to 1.5. These results are in agreement with the experiments of Palandri and Kharaka [63] that indicate a comparable increase of forsterite dissolution rate from $10^{-10.5}$ to $10^{-8.5}$ (mol/m^2/s) for pH values ranging from 7.3 to 2. Dissolution of augite vs. pH follows similar trends, ranging from 10^{-12} to $10^{-8.5}$ (mol/m^2/s) for the same pH range with augite (Figure 5b). Experimental results suggest that dissolution rate of diopside will be three orders of magnitude slower compared to other silicate

minerals, such as olivine at 25 °C [69,70]. Data provided by Palandri and Kharaka [63] point to an increase of the plagioclase dissolution rate from $10^{-11.5}$ to 10^{-10} (mol/m^2/s) for pH values ranging from 7 to 2.

Dissolution rate of CO_2 in water strongly depends on the water temperature, the partial pressure of CO_2, and the salinity of the medium [50]. Carbonation rate of secondary minerals is strongly associated with the acidic or alkaline nature of the water. Experimental results at a temperature of 25 °C under acidic and neutral conditions show that the carbonation rate of calcite, magnesite, and siderite ranges are $10^{-0.3}$–$10^{-5.81}$ mol/(m^2/s) [63], $10^{-6.38}$–$10^{-9.34}$ mol/(m^2/s) [63], and $10^{-3.74}$–$10^{-8.90}$ mol/(m^2/s) [71], respectively. This further suggests that precipitation of carbonate minerals is mostly favoured during the late stages of the CO_2 injection, characterised by lower pH values compared to the formation groundwater (pH: 7.3 for Microthives groundwater). Availability of divalent cations is the main limiting step during CO_2 mineralisation in basalts [5]. Basalts of 8% average MgO correspond to 0.087 CO_2 g/g basalt converted to magnesite [3]. Abundance of Mg-olivine in the studied basalts from the regions of Microthives and Porphyrio support their high potential for magnesite precipitation. The relatively low alteration grade of the studied basalts provides additional advantages regarding their potential for mineral carbonation, due to their higher carbonation grades compared to the altered ones [72].

4.2. Groundwater Chemistry from Irrigation Wells

Chemical comparison between the groundwater samples from the studied localities indicate that shallow groundwater is more depleted in Cl^- and Na^+ compared to the deep one. Cl^- is a relatively mobile element that does not incorporate into secondary minerals after being released from the dissolution of the basaltic protolith [51]. The different Cl^- contents between the analysed borehole groundwater samples are attributed to their distance from seawater [73], origin, and circulation. In particular, the sampling site of the deep groundwater is located closer to the Aegean Sea compared to the shallow one. The aforementioned difference is attributed to the mixture between the deep groundwater from Microthives and seawater and confirmed by the ionic ratios (Table 3), coupled with the Langelier–Ludwig [74] and Piper plots [46] (Figure 6a,b). The shallow groundwater presents similar Na–Cl contents compared to those of the groundwater from Iceland (Figure 6a). This suggests that both water samples were not affected by mixture processes with seawater.

Table 3. Ionic ratios of water samples from the region of Microthives (mg/L) [28].

Ionic Ratio	Mg/Ca	Na/K	Na/Cl	SO_4^{2-}/Cl^-	HCO_3^-/Cl^-	Cl^-/F	Cl^-/Br	Cl/Li	Na/Li
Deep sample	0.75	35.78	0.49	0.15	1.74	369	77.0	6600	3220
Shallow sample	1.68	13.54	0.90	0.50	22.41	57.0	57.0	2167	62,583
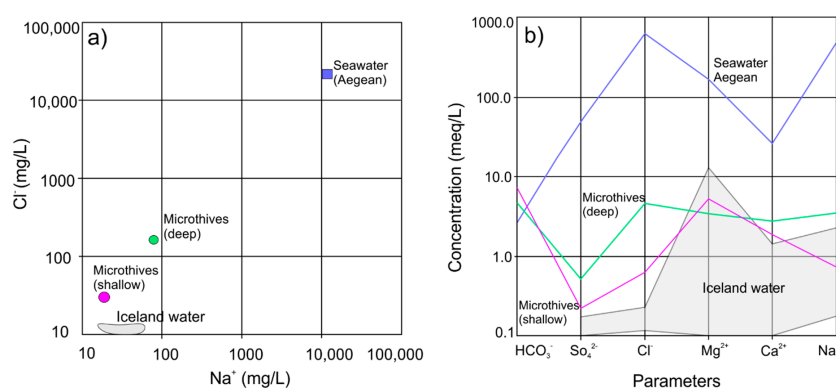
Figure 6. (**a**) Ludwig–Langelier [74] diagram for the water sample of Microthives and the seawater sample from the Aegean Sea. (**b**) Schoeller diagram [75] for the Microthives water sample and the Aegean seawater [28,51].

The groundwater composition is also affected by the water–rock interaction during the circulation of rainwater through basalts [51].

4.3. Indications of Enhanced Heat

Volcanic rocks in the Porphyrio and Microthives localities were developed in an extensional back-arc geotectonic setting affected by the activity of the Northern Anatolian Fault [19–21]. This back-arc extension was evolved with respect to the active volcanic arc of the South Aegean [21] and gave rise to the generation of Late Pleistocene basalts. The age of the magmatism is very crucial to the determination of the heat source [76]. In particular, the active magmatism is indicative of elevated heat sources, compared to the inactive or extinct magmatism that are associated with heat remnants and/or additional radioactive-heat [76,77].

The back-arc extension developed in Porphyrio and Microthives localities indicates a recent-inactive enhanced heat, characterised by the development of relatively shallow and young magma chambers [76]. These systems are mainly developed in divergent plate margins [76], usually including two distinct zones of different T and pH conditions [76,78–80]. In particular, the outflow zone has a lower T and neutral-to-alkaline pH groundwaters [80] compared to the upflow, which is more acidic [81]. In the cases of inactive magmatic sources, the produced heat is strongly associated with crystallised, but still-cooling, magmatic bodies [76]. According to this model, the main heat source is provided by the Pleistocene magmatic melts, whereas the presence of faults further enhances the recharge of meteoric waters [76]. A similar heating source was developed in Hungary as a result of a Miocene extension that caused a high thermal attenuation of the lithosphere [82,83]. In the current study, the elevated water temperatures were mainly observed close to the basaltic rock occurrences (T = 30.2 and 23.0 °C for GTES-038 and GTES-040 groundwater irrigations wells, respectively). Enhanced water temperatures are also recorded in the adjacent regions of Kamena Vourla (Central Greece; East Thessaly) and Lichades islands (Central Greece; North Evoikos Gulf), corresponding to 25–41.3 °C and 41 °C, respectively [84]. These regions are related to scattered volcanic centers, which were active during the Late Pleistocene–Quaternary period, similarly to those of the Porphyrio and Microthives localities. The above data suggest that this activity is associated with the extensional back-arc tectonic setting. Based upon the geological mapping of the Porphyrio and Microthives localities, coupled with the elevated temperatures of the groundwater samples (irrigation wells GTES-038 and GTES-040), the elevated temperatures in the studied region are strongly associated with the basalt occurrence underneath the Neogene alluvial sediments. The water pH in the Microthives locality (pH: 7.20–7.30; [28]) and the adjacent regions of Kamena Vourla and Aidipsos (pH: 6.28 and 6.80 respectively; [85]) indicate that these waters are derived from the outflow zone, which is characterised by a neutral-to-alkaline pH [81].

4.4. A Case Scenario for Mineral Carbonation in the Micothives Basalts

The Microthives and Porphyrio basaltic occurrences are potential sites for CO_2 storage [86]. The research area is located 10 km away from the industrial zone of Volos, a significant source of CO_2 emissions. The case study scenario presented in this study is based on the results of the CarbFix project [50,55]. Carbon storage through injection of water dissolved CO_2, is a potential applicable CCS scenario for the volcanic rocks of Microthives and Porphyrio localities.

The CarbFix method does not require the presence of a cap rock, since the dissolved CO_2 is not buoyant [55]. The process of CO_2 dissolution during the injection into basaltic rocks [55] of the Microthives and Porphyrio localities, can be enhanced due to the higher porosity that these rocks present (average porosity: 18%). There is a strong association between the porosity and permeability of the basaltic rocks and their alteration grade [55]. Thus, the younger and less-altered basalts are more appropriate for CO_2 storage compared to the older types. Basaltic rocks of the current study belong to the relatively young extensional Pleistocene volcanic activity, and, hence, they were not affected by a high alteration grade. The pH value in the groundwater from the Microthives locality is

7.3, which is similar to that of the target zone prior to the injection of CO_2 in the CarbFix project [10,50]. After the initial pH decrease, due to the mixing of the groundwater fluids with the hydrous injected CO_2, the reaction paths of basaltic glass at 25 °C [51] indicate that pH becomes more alkaline due to the P_{CO_2} decrease during the water–rock interaction.

Regarding the diffusivity of water-dissolved CO_2 in basalts, we provide preliminary calculations with Equation (12) [87]:

$$D = D_0 \cdot \varphi^{m} \tag{12}$$

where D is diffusion coefficient; D_0 is diffusion of the water dissolved CO_2, ($1.92 \cdot 10^{-5}$ cm^2/s [88]; φ is porosity of basalt (0.18–0.23 for our studied basalts); and m is Archie's coefficient, (m: 2.3 [89]). By applying the aforementioned equation, it is estimated the diffusion coefficient ranges from $38 \times \cdot 10^{-8}$ cm^2/s to 65×10^{-8} cm^2/s, respectively.

One of the major parameters in the CarbFix project is the substantial quantities of water for the dissolution of CO_2 during injection [50]. Basaltic outcrops of Microthives–Porphyrio localities are in proximity with the Aegean Sea, giving the potential for high storage capacities, due to the unlimited seawater supply [6,50,90,91].

We provide preliminary calculations that estimate the CO_2 that could be stored in the frames of pilot projects for the two basalt locations of Microthives and Porphyrio. For this purpose, we apply the function below:

$$\text{Storage Capacity } = \sum (V \times \varphi \times \rho \times \varepsilon) \tag{13}$$

where V is the volume of the basaltic outcrop; φ is the average porosity = 18%; ρ is the specific gravity of the sCO_2; and ε is the sCO_2 storage ratio.

The Microthives basaltic outcrop has a surface of ~8 km^2; therefore, the potential pilot project can be realised at an estimated volume of 300 m (length) × 200 m (width) × 300 m (depth) = 18×10^6 m^3. Taking into consideration the average porosity of basalts from our studied site (18%), the specific gravity of the scCO$_2$ (400 kg/m^3; at 10 MPa and 50 °C [92,93]), and the scCO$_2$ storage ratio of basalts (5% [94]), the Microthives basaltic outcrop could store an amount of 64,800 tons of CO_2. The Porphyrio basaltic formation is smaller, and, therefore, by assuming an estimated volume of 200 m (length) × 100 m (width) × 300 m (depth) = 6×10^6 m^3, it could store a calculated amount of 21,600 tons of CO_2. The maximum capability of CO_2 storage, considering the highest porosity of the studied suite (23%), corresponds to 82,800 tons and 27,600 tons for the Microthives and Porphyrio basalts, respectively. The size of these outcrops could serve for storage of much larger amounts of CO_2 after deployment of pilot tests.

The charged water can significantly increase the energy consumed for the CO_2 injection. From the CarbFix experience, it is evident that the cost of storage and transport corresponds to \$17/ton of dissolved CO_2 injected [50,95], which doubles the cost compared to the classic CO_2 injection in sedimentary basins [50,96]. This cost is balanced by the lower monitoring after the injection period, due to the non-buoyant nature of the mineralised CO_2 [50]. The development of a cost-effective scenario is further enhanced by the relatively short distance of the basaltic dominated areas (~10 km) from the industrial area of Volos, reducing the cost of transport.

5. Conclusions

Pleistocene volcanic rocks are present in the region of Volos (Central Greece) and in the specific localities of Microthives and Porphyrio. They are classified as basaltic and trachyandesitic lavas and were formed due to back-arc extension of the Aegean Sea. Their geochemical affinities suggest that these are alkaline basalts of OIB affinity. Results from detailed petrographic examination show that their porosity ranges between 5% and 40% with vesicles, which, in a few rock samples, partly host calcite. The vast majority of the studied samples exhibit porosity that ranges between 15% and 23%.

A recent-inactive magmatic heating source present in the Microthives basaltic vicinity, affected the groundwater temperature regime. Enhanced groundwater temperatures are also recorded in adjacent

regions with basalts of similar composition and age, suggesting that this activity is associated with the extensional back-arc tectonic setting. Deep and shallow groundwater samples are classified as Ca-Mg-Na-HCO$_3$-Cl and the Mg-HCO$_3$ hydrochemical types respectively. Measured groundwater temperatures from irrigation wells, at depths between 170 and 250 m, reach up to ~30 °C.

Basalts from the region of Volos have the necessary appropriate physicochemical features to be considered as potential sites for implementing carbon capture and storage (CCS) technologies due to (i) low alteration grade, (ii) silica-undersaturated alkaline composition, (iii) presence of Ca-bearing minerals, (iv) high porosity, and (v) indications of enhanced heat. The proximity of the basaltic rocks to the sea gives the opportunity for exploitation of the unlimited water sources during the CO$_2$ injection. Furthermore, these outcrops are in close distance to the industrial area of Volos, providing the potential for the development of a financially feasible scenario. Preliminary calculations suggest that potential pilot projects at the Microthives and Porphyrio basaltic formations can store 82,800 and 27,600 tons of maximum CO$_2$, respectively, although their size could serve for storage of much larger amounts of CO$_2$ after deployment of pilot tests. Further and detailed petrological, petrophysical, geochemical, hydrochemical, geothermal, and financial research studies are needed prior to deployment of pilot tests in the region of Volos.

Author Contributions: All authors actively participated in a balanced manner at all stages of the research presented in this paper. This involved participation of all authors in sample collection in the field, performing laboratory work and manuscript writing.

Conflicts of Interest: The authors declare no conflict of interest.

References

1. IPCC. Intergovernmental Panel. In *Climate Change 2013 the Physical Science Basis*; Cambridge University Press: New York, NY, USA, 2013.
2. Davis, W.J. The Relationship between Atmospheric Carbon Dioxide Concentration and Global Temperature for the Last 425 Million Years. *Climate* **2017**, *5*, 76–110.
3. Rosenbauer, R.J.; Thomas, B.; Bischoff, J.L.; Palandri, J. Carbon sequestration via reaction with basaltic rocks: Geochemical modeling and experimental results. *Geochim. Cosmochim. Acta* **2012**, *89*, 116–133. [CrossRef]
4. Adam, L.; Otheim, T.; van Wijk, K.; Batzle, M.; McLing, T.L.; Podgorney, R.K. CO$_2$ Sequestration in Basalt: Carbonate Mineralization and Fluid Substitution. In *SEG Technical Program Expanded Abstracts 2011*; Society of Exploration Geophysicists: Tulsa, OK, USA, 2011; pp. 2108–2113.
5. Oelkers, E.H.; Gislason, S.R.; Matter, J. Mineral carbonation of CO$_2$. *Elements* **2008**, *4*, 333–337. [CrossRef]
6. Gislason, S.R.; Wolff-Boenisch, D.; Stefansson, A.; Oelkers, E.H.; Gunnlaugsson, E.; Sigurdardottir, H.; Sigfusson, B.; Broecker, W.S.; Matter, J.M.; Stute, M. Mineral sequestration of carbon dioxide in basalt: A pre-injection overview of the CarbFix project. *Int. J. Greenh. Gas Control* **2010**, *4*, 537–545. [CrossRef]
7. Koukouzas, N.; Kypritidou, Z.; Purser, G.; Rochelle, C.A.; Vasilatos, C.; Tsoukalas, N. Assessment of the impact of CO$_2$ storage in sandstone formations by experimental studies and geochemical modeling: The case of the Mesohellenic Trough, NW Greece. *Int. J. Greenh. Gas Control* **2018**, *71*, 116–132. [CrossRef]
8. Black, J.R.; Carroll, S.A.; Haese, R.R. Rates of mineral dissolution under CO$_2$ storage conditions. *Chem. Geol.* **2015**, *399*, 134–144.
9. Gaus, I. Role and impact of CO$_2$—Rock interactions during CO$_2$ storage in sedimentary rocks. *Int. J. Greenh. Gas Control* **2010**, *4*, 73–89. [CrossRef]
10. Kelektsoglou, K. Carbon capture and storage: A review of mineral storage of CO$_2$ in Greece. *Sustainability* **2018**, *10*, 4400. [CrossRef]
11. Saccani, E.; Photiades, A. Mid-ocean ridge and supra–subduction affinities in the Pindos ophiolites (Greece): Implications for magma genesis in a forearc setting. *Lithos* **2004**, *73*, 229–253. [CrossRef]

12. Stouraiti, C.; Pantziris, I.; Vasilatos, C.; Kanellopoulos, C.; Mitropoulos, P.; Pomonis, P.; Moritz, R.; Chiaradia, M. Ophiolitic remnants from the upper and intermediate structural unit of the Attic-Cycladic Crystalline Belt (Aegean, Greece): Fingerprinting geochemical affinities of magmatic precursors. *Geosciences* **2017**, *7*, 14. [CrossRef]

13. Mortazavi, M.; Sparks, R. Origin of rhyolite and rhyodacite lavas and associated mafic inclusions of Cape Akrotiri, Santorini: The role of wet basalt in generating calcalkaline silicic magmas. *Contrib. Miner. Pet.* **2004**, *146*, 397–413. [CrossRef]

14. Bachmann, O.; Deering, C.D.; Ruprecht, J.S.; Huber, C.; Skopelitis, A.; Schnyder, C. Evolution of silicic magmas in the Kos-Nisyros volcanic center, Greece: A petrological cycle associated with caldera collapse. *Contrib. Miner. Pet.* **2012**, *163*, 151–166. [CrossRef]

15. Pomonis, P.; Tsikouras, V.; Hatzipanagiotou, K. Geological evolution of the Koziakas ophiolitic complex (W. Thessaly, Greece). *Ofioliti* **2005**, *30*, 77–86.

16. Koutsovitis, P. Gabbroic rocks in ophiolitic occurrences from East Othris, Greece: Petrogenetic processes and geotectonic environment implications. *Miner. Pet.* **2012**, *104*, 249–265. [CrossRef]

17. Pe-Piper, G.; Panagos, A.G. Geochemical characteristics of the Triassic volcanic rocks of Evia: Petrogenetic and tectonic implications. *Ofioliti* **1989**, *14*, 33–50.

18. Saccani, E.; Beccaluva, L.; Photiades, A.; Zeda, O. Petrogenesis and tectono-magmatic significance of basalts and mantle peridotites from the Albanian—Greek ophiolites and sub-ophiolitic mélanges. New constraints for the Triassic—Jurassic evolution of the Neo-Tethys in the Dinaride sector. *Lithos* **2011**, *124*, 227–242. [CrossRef]

19. Fytikas, M.; Innocenti, F.; Manetti, P.; Mazzuoli, R.; Peccerillo, A.; Villari, L. Tertiary to Quaternary evolution of volcanism in the Aegean region. In *The Geological Evolution of the Eastern Mediterranean*; Dixon, J.E., Robertson, A.H.F., Eds.; Geological Society Special Publications: London, UK, 1984; Volume 17, pp. 687–699.

20. Pe–Piper, G.; Piper, D.J. *Neogene Backarc Volcanism of the Aegean: New Insights into the Relationship between Magmatism and Tectonics*; Special Papers; Geological Society of America: Boulder, CO, USA, 2007; p. 17.

21. Innocenti, F.; Agostini, S.; Doglioni, C.; Manetti, P.; Tonarini, S. Geodynamic evolution of the Aegean: Constraints from the Plio-Pleistocene volcanism of the Volos–Evia area. *J. Geol. Soc. Lond.* **2010**, *167*, 475–489. [CrossRef]

22. Katsikatsos, G.; Mylonakis, J.; Vidakis, M.; Hecht, J.; Papadheas, G.; Dimou, E.; Papazeti, E.; Skourtsi-Koroneou, V.; Hadjicostanti–Tsalachouri, I.; Karamicahlou–Kavali, A.; et al. *Geological Map of Greece, Volos Sheet*; Institute of Geology and Mineral Exploration of Greece: Athens, Greece, 1978.

23. Katsikatsos, G.; Mylonakis, J.; Triantaphyllis, E.; Papadheas, G.; Psonis, C.; Staila-Monopolis, S.; Skourtsi–Coroneou, V.; Hadjicostani-Tsalachouri, I.; Georgiou-Nikolaidi, A.; Benaki-Dragoumanou, E.; et al. *Geological Map of Greece, Velestino Sheet*; Institute of Geology and Mineral Exploration of Greece: Athens, Greece, 1978.

24. Katsikatsos, G.H. *Geology of Greece*; University Publications: Patra, Greece, 1992; p. 451.

25. Papanikolaou, D. Timing of tectonic emplacement of the ophiolites and terrane paleogeography in the Hellenides. *Lithos* **2009**, *108*, 262–280. [CrossRef]

26. Pe–Piper, G.; Piper, D.J.W. *The Igneous Rocks of Greece: The Anatomy of an Orogen*; Gebrüder Borntraegen: Berlin/Stuttgart, Germany, 2002.

27. Rigopoulos, I.; Vasiliades, M.A.; Ioannou, I.; Efstathiou, A.M.; Godelitsas, A.; Kyratsi, T. Enhancing the rate of ex situ mineral carbonation in dunites. *Adv. Powder Technol.* **2016**, *27*, 360–371. [CrossRef]

28. Vakalopoulos, P.; Efthimiopoulos, T.; Arvanitis, A.; Xenakis, M.; Vougioukalakis, G.; Galamakis, D.; Gkagka, M.; Lachana, G.; Kanellopoulos, C.; Fragkogiannis, G.; et al. Geothermal exploration in Eastern Thessaly. I.G.M.E., NSRF (National Strategic Reference Framework) 2007–2013/Operational Programme "Competitiveness and Entrepreneurship"/Project "Geothermal energy exploration in selected areas, in order to reduce energy dependency and environmental impact. Assessment of hot groundwater and geothermal resources (GEOTHEN)". Athens, Greece, 2016; p. 238. Available online: http://igme.gr/index.php/proionta-ypiresies/23-erga/erga-espa-2007-2013 (accessed on 15 May 2016).

29. Pe–Piper, G.; Piper, D.J.W. Plio–Pleistocene ages of high-potassium volcanism in the northwestern part of the Hellenic arc. *Tschermaks Mineral. Petrogr. Mitt.* **1979**, *26*, 163–165. [CrossRef]

30. Ninkovich, D.; Hays, J.D. Mediterranean island arcs and origin of high potash volcanoes. *Earth Planet. Sci. Lett.* **1972**, *16*, 331–345. [CrossRef]

31. Pe, G.; Panagos, A. Comparative geochemistry of the Northern Eubeoecos lavas. *Bull. Geol. Soc. Greece* **1976**, *9*, 95–130, (In Greek with English Abstract).

32. Weaver, B.L. The origin of ocean island basalt end-member compositions: Trace element and isotopic constraints. *Earth Planet. Sci. Lett.* **1991**, *104*, 381–397. [CrossRef]

33. Pe, G.G. Petrology and geochemistry of volcanic rocks of Aegina, Greece. *Bull. Volcanol.* **1973**, *37*, 491–514. [CrossRef]

34. Wyers, G.P.; Barton, M.D. Geochemistry of a transitional Ne-trachybasalt-Q-trachyte lava series from Patmos (Dodecanesos), Greece: Further evidence for fractionation, mixing and assimilation. *Contrib. Miner. Pet.* **1987**, *97*, 279–291. [CrossRef]

35. Huijsmans, J.P.P.; Barton, M.D.; Salters, V.J.M. Geochemistry and evolution of the calc-alkaline volcanic complex of Santorini, Aegean Sea. *J. Volcanol. Geotherm. Res.* **1988**, *34*, 283–306. [CrossRef]

36. Druitt, T.H.; Mellors, R.A.; Pyle, D.M.; Sparks, R.S.J. Explosive volcanism on Santorini, Greece. *Geol. Mag.* **1989**, *126*, 95–126. [CrossRef]

37. Nicholls, I.A. Petrology of Santorini volcanic rocks. *J. Pet.* **1971**, *12*, 67–119. [CrossRef]

38. Nicholls, I.A. Santorini volcano, Greece. Tectonic and petrochemical relationships with volcanics of the Aegean region. *Tectonophysics* **1971**, *11*, 377–385. [CrossRef]

39. Pe, G.G.; Piper, D.J.W. Vulcanism at subduction zones; The Aegean area. *Bull. Geol. Soc. Greece* **1972**, *9*, 113–144.

40. Le Maitre, R.W. *Igneous Rocks—A Classification and Glossary of Terms*; Cambridge University Press: Cambridge, UK, 2002.

41. Mcdonough, W.F.; Sun, S.S. The composition of the Earth. *Chem. Geol.* **1995**, *120*, 223–253. [CrossRef]

42. Sun, S.S.; McDonough, W.F. Chemical and isotopic systematics of oceanic basalts; implications for mantle composition and processes. In *Magmatism in the Ocean Basins*; Saunders, A.D., Norry, M.J., Eds.; The Geological Society by Blackwell Scientific Publications: London, UK, 1989; Volume 42, pp. 313–345.

43. Castany, G. *Traité Pratique des Eaux Souterraines*; Dunod: Paris, France, 1963.

44. Hem, J.D. *Study and Interpretation of the Chemical Characteristics of Natural Water*, 2nd ed.; (Water Supply Paper); U.S. Government Printing Office: Washington, WA, USA, 1970.

45. Sawyer, C.N.; McCarty, P.L. *Chemistry and Sanitary Engineers*; McGrawHall: New York, NY, USA, 1966.

46. Piper, A.M. A graphic procedure in the geochemical interpretation of water analyses. *Trans. Am. Geophys. Union.* **1944**, *25*, 914–928. [CrossRef]

47. Xenakis, M.; Kavouridis, T.; Vrellis, G.; Vakalopoulos, P. *Exploration and Identification of Geothermal Fields on Chios Island*; Institute of Geology and Mineral Exploration of Greece (I.G.M.E.), Department of Geothermal Energy and Thermometallic Waters: Athens, Greece, 2007.

48. Dessert, C.; Dupré, B.; Gaillardet, J.; François, L.M.; Allegre, C.J. Basalt weathering laws and the impact of basalt weathering on the global carbon cycle. *Chem. Geol.* **2003**, *202*, 257–273. [CrossRef]

49. McGrail, B.P.; Schaef, H.T.; Ho, A.M.; Chien, Y.J.; Dooley, J.J.; Davidson, C.L. Potential for carbon dioxide sequestration in flood basalts. *J.Geophys. Res. Solid Earth* **2006**, *111*. [CrossRef]

50. Gislason, S.R.; Broecker, W.S.; Gunnlaugsson, E.; Snæbjörnsdóttir, S.; Mesfin, K.G.; Alfredsson, H.A.; Aradottir, E.S.; Sigfusson, B.; Gunnarsson, I.; Stute, M.; et al. Rapid solubility and mineral storage of CO_2 in basalt. *Energy Procedia* **2014**, *63*, 4561–4574. [CrossRef]

51. Alfredsson, H.A.; Oelkers, E.H.; Hardarsson, B.S.; Franzson, H.; Gunnlaugsson, E.; Gislason, S.R. The geology and water chemistry of the Hellisheidi, SW-Iceland carbon storage site. *Int. J. Greenh. Gas Control* **2013**, *12*, 399–418. [CrossRef]

52. Schaef, H.T.; McGrail, B.P.; Owen, A.T. Carbonate mineralization of volcanic province basalts. *Int. J. Greenh. Gas Control* **2010**, *4*, 249–261. [CrossRef]

53. Rigopoulos, I.; Petallidou, K.C.; Vasiliades, M.A.; Delimitis, A.; Ioannou, I.; Efstathiou, A.M.; Kyratsi, T. Carbon dioxide storage in olivine basalts: Effect of ball milling process. *Powder Technol.* **2015**, *273*, 220–229. [CrossRef]

54. Gerdemann, S.K.; O'Connor, W.K.; Dahlin, D.C.; Panner, L.R.; Rush, H. Ex situ aqueous mineral carbonation. *Environ. Sci. Technol.* **2007**, *41*, 2587–2593. [CrossRef]

55. Snæbjörnsdóttir, S.Ó.; Wiese, F.; Fridriksson, T.; Ármansson, H.; Einarsson, G.M.; Gislason, S.R. CO_2 storage potential of basaltic rocks in Iceland and the oceanic ridges. *Energy Procedia* **2014**, *63*, 4585–4600.

56. Teir, S.; Kuusik, R.; Fogelholm, C.-J.; Zevenhoven, R. Production of magnesium carbonates from serpentinite for long–term storage of CO_2. *Int. J. Miner. Process.* **2007**, *85*, 1–15. [CrossRef]

57. Koukouzas, N.; Ziogou, F.; Gemeni, V. Preliminary assessment of CO_2 geological storage opportunities in Greece. *Int. J. Greenh. Gas Control* **2009**, *3*, 502–513. [CrossRef]

58. Hähnchen, M.; Prigiobbe, V.; Storti, G.; Seward, T.M.; Mazzotti, M. Dissolution kinetics of fosteritic olivine at 90–150 degrees C including effects of the presence of CO_2. *Geochim. Cosmochim. Acta* **2006**, *70*, 4403–4416. [CrossRef]

59. Zhang, P.C.; Anderson, H.L.; Kelly, J.W.; Krumhansl, J.L.; Papenguth, H.W. *Kinetics and Mechanisms of Formation of Magnesite from Hydromagnesite in Brine United States*; Department of Energy, US Department of Energy, Sandia National Labs.: Albuquerque, NM, USA; Livermore, CA, USA, 2000; pp. 1–26.

60. Clark, D.E.; Gunnarsson, I.; Aradóttir, E.S.; Arnarson, M.Þ.; Þorgeirsson, Þ.A.; Sigurðardóttir, S.S.; Sigfússon, B.; Snæbjörnsdóttir, S.Ó.; Oelkers, E.H.; Gíslason, S.R. The chemistry and potential reactivity of the CO_2-H_2S charged injected waters at the basaltic CarbFix2 site, Iceland. *Energy Procedia* **2018**, *146*, 121–128. [CrossRef]

61. Franzson, H. Reservoir Geology of the Nesjavellir High-Temperature Field in SW-Iceland. In Proceedings of the 19th Annual PNOC—EDC Geothermal Conference, Manila, Philippines, 5–6 March 1998; pp. 13–20.

62. Tómasson, J.; Kristmannsdóttir, H. High temperature alteration minerals and thermal brines, Reykjanes, Iceland. *Contrib. Miner. Pet.* **1972**, *36*, 132–134. [CrossRef]

63. Palandri, J.L.; Kharaka, Y.K. *A Compilation of Rate Parameters of Water-Mineral Interaction Kinetics for Application to Geochemical Modeling*; U.S. Geological Survey Open File Report (of 2004-1068); National Energy Technology Laboratory—United States Department of Energy: Menlo Park, CA, USA, 2004; p. 71.

64. Pokrovsky, O.S.; Schott, J. Forsterite surface composition in aqueous solutions: A combined potentiometric, electrokinetic, and spectroscopic approach. *Geochim. Cosmochim. Acta* **2000**, *64*, 3299–3312. [CrossRef]

65. Oelkers, E.; Gislason, S. The mechanism, rates and consequences of basaltic glass dissolution: I. An experimental study of the dissolution rates of basaltic glass as a function of aqueous Al, Si and oxalic acid concentration at 25 °C and pH = 3 and 11. *Geochim. Cosmochim. Acta* **2001**, *65*, 3671–3681. [CrossRef]

66. Knauss, K.; Nguyen, S.; Weed, H. Diopside dissolution kinetics as a function of pH, CO_2, temperature, and time. *Geochim. Cosmochim. Acta* **1993**, *57*, 285–294. [CrossRef]

67. Gudbrandsson, S.; Wolff-Boenisch, D.; Gislason, S.; Oelkers, E. Experimental determination of plagioclase dissolution rates as a function of its composition and pH at 22 °C. *Geochim. Cosmochim. Acta* **2014**, *139*, 154–172. [CrossRef]

68. Pollyea, R.M.; Rimstidt, J.D. Rate equations for modeling carbon dioxide sequestration in basalt. *Appl. Geochem.* **2017**, *81*, 53–62. [CrossRef]

69. De Paolo, D.J.; Cole, D.R.; Navrotsky, A.; Bourg, I.C. Geochemistry of Geologic CO_2 Sequestration. *Mineral. Soc. Am.* **2013**, *77*, 536.

70. Kaszuba, J.; Yardley, B.; Andreani, M. Experimental perspectives of mineral dissolution and precipitation due to carbon dioxide-water-rock interactions. *Rev. Mineral. Geochem.* **2013**, *77*, 153–188. [CrossRef]

71. Golubev, S.V.; Bénézeth, P.; Schott, J.; Dandurand, J.L.; Castillo, A. Siderite dissolution kinetics in acidic aqueous solutions from 25 to 100 °C and 0 to 50 atm p CO_2. *Chem. Geol.* **2009**, *265*, 13–19. [CrossRef]

72. Liu, D.; Agarwal, R.; Li, Y.; Yang, S. Reactive transport modeling of mineral carbonation in unaltered and altered basalts during CO_2 sequestration. *Int. J. Greenh. Gas Control* **2019**, *85*, 109–120. [CrossRef]

73. Sigurdsson, F.; Einarsson, K. Groundwater resources of Iceland—Availability and demand. *Jökull* **1988**, *38*, 35–53.

74. Langelier, W.F.; Ludwig, H.F. Graphical Methods for Indicating the Mineral Character of Natural Waters. *J. Am. Water Works Assn.* **1942**, *34*, 335–352. [CrossRef]

75. Schoeller, H. Geochimie deseaux souterraines. *Rev. Inst. Franc. Pètrole. Paris* **1955**, *10*, 181–213.

76. World Bank. *Best Practices Guide for Geothermal Exploration*; Bochum University of Applied Sciences: Bochum, Germany, 2014; p. 196.

77. McCoy-West, A.; Milicich, S.; Robinson, T.; Bignall, G.; Harvey, C.C. Geothermal resources in the Pacific Islands: The potential of power generation to benefit indigenous communities. In Proceedings of the 36th Workshop on Geothermal Reservoir Engineering, Stanford University, Stanford, CA, USA, 31 January–2 February 2011.

78. Williams, C.F.; Reed, M.J.; Anderson, A.F. Updating the classifi cation of geothermal resources. In Proceedings of the hirty-Sixth Workshop on Geothermal Reservoir Engineering Stanford University, Stanford, CA, USA, 31 January–2 February 2011; p. 7.

79. Giggenbach, W.F. Magma degassing and mineral deposition in hydrothermal systems along convergent plate boundaries. *Econ. Geol. Soc. Explor. Geol. Bull.* **1992**, *97*, 1927–1944.

80. Hochstein, M.P. Assessment and modelling of geothermal reservoirs (small utilization schemes). *Geothermics* **1988**, *17*, 35. [CrossRef]

81. Moeck, I.S. Catalog of geothermal play types based on geologic controls. *Renew. Sustain. Energ. Rev.* **2014**, *37*, 867–882. [CrossRef]

82. Horváth, F. Towards a mechanical model for the formation of the Pannonian basin. *Tectonophysics* **1993**, *226*, 333–357. [CrossRef]

83. Békési, E.; Lenkey, L.; Limberger, J.; Porkoláb, K.; Balázs, A.; Bonté, D.; Vrijlandt, M.; Horváth, F.; Cloetingh, S.; van Wees, J.-D. Subsurface temperature model of the Hungarian part of the Pannonian Basin. *Glob. Planet. Chang.* **2018**, *171*, 48–64. [CrossRef]

84. Andritsos, N.; Arvanitis, A.; Papachristou, M.; Fytikas, M.; Dalambakis, P. Geothermal Activities in Greece During 2005–2009. In Proceedings of the World Geothermal Congress 2010, Bali, Indonesia, 25–29 April 2010.

85. Baba, A.; Bundschuh, J.; Chandrasekharam, D. *Geothermal Systems and Energy Resources: Turkey and Greece*, 1st ed.; CRC Press/Balkema: Boca Raton, FL, USA, 2014; p. 291.

86. Koutsovitis, P.; Koukouzas, N.; Magganas, A. Carbon Storage Potential in Pleistocene Volcanic Rocks of the Magnesia Area (Central Greece). In Proceedings of the 19th EGU General Assembly EGU2017, Vienna, Austria, 23–28 April 2017; p. 3942.

87. Navarre–Sitchler, A.; Steefel, C.I.; Yang, L.; Tomutsa, L.; Brantley, S.L. Evolution of porosity and diffusivity associated with chemical weathering of a basalt clast. *J. Geophys. Res. Earth Surf.* **2009**, *114*. [CrossRef]

88. Cussler, E.L. *Diffusion: Mass Transfer in Fluid Systems*; Cambridge University Press: New York, NY, USA, 1997; p. 580.

89. Peng, S.; Hu, Q.; Hamamoto, S. Diffusivity of rocks: Gas diffusion measurements and correlation to porosity and pore size distribution. *Water Resour. Res.* **2012**, *48*. [CrossRef]

90. Wolff–Boenisch, D.; Wenau, S.; Gislason, S.R.; Oelkers, E.H. Dissolution of basalts and peridotite in seawater, in the presence of ligands, and CO_2: Implications for mineral sequestration of carbon dioxide. *Geochim. Cosmochim. Acta* **2011**, *75*, 5510–5525. [CrossRef]

91. Goldberg, D.S.; Takahashi, T.; Slagle, A.L. Carbon dioxide sequestration in deep-sea basalt. *Proc. Natl. Acad. Sci. USA* **2008**, *105*, 9920–9925. [CrossRef] [PubMed]

92. Span, R.; Wagner, W. A new equation of state for carbon dioxide covering the fluid region from the triple-point temperature to 1100 K at pressures up to 800 MPa. *J. Phys. Chem. Ref. Data* **1996**, *25*, 1509–1596. [CrossRef]

93. Spycher, N.; Pruess, K. CO_2-H_2O mixtures in the geological sequestration of CO_2. II. Partitioning in chloride brines at 12–100 °C and up to 600 bar. *Geochim. Cosmochim. Acta* **2005**, *69*, 3309–3320. [CrossRef]

94. Gislason, S.; Oelkers, E. Carbon Storage in Basalt. *Science* **2014**, *344*, 373–374. [CrossRef]

95. Ragnheidardottir, E.; Sigurdardottir, H.; Kristjansdottir, H.; Harvey, W. Opportunities and challenges for CarbFix: An evaluation of capacities and costs for the pilot scale mineralization sequestration project at Hellisheidi, Iceland and beyond. *Int. J. Greenh. Gas Control* **2011**, *5*, 1065–1072. [CrossRef]

96. Global CCS Institute. *Economic Assessment of Carbon Capture and Storage Technologies*; Global CCS Institute: Canberra, Australia, 2011.